Modeling the response to changes in tropospheric methane concentration: Application to the Permian-Triassic boundary

J.-F. Lamarque,[1] J. T. Kiehl,[1] C. A. Shields,[1] B. A. Boville,[1] and D. E. Kinnison[1]

Received 23 January 2006; revised 31 March 2006; accepted 25 April 2006; published 9 August 2006.

[1] We discuss model experiments valid for the Permian-Triassic boundary in which we explore the impact of changes in tropospheric methane concentration. For scenarios relevant to methane clathrate release, we consider surface methane concentration with values up to 5000 times its preindustrial concentration. We employ a comprehensive three-dimensional tropospheric-stratospheric model with chemistry that allows for the feedbacks between chemistry and climate. We show that stratospheric ozone starts collapsing for methane surface concentrations on the order of 1000 times their preindustrial concentration. At 5000 times, more than half of the total ozone column has disappeared. As a result a large rise (up to a factor of 7) in surface UV-B radiation is found. Other chemical consequences include a rise in CO and ozone surface concentrations; although becoming very large (up to 17 ppmv for CO), neither seems to reach lethal values according to present-day life forms. Finally, we show that tropospheric OH does not collapse for any of the scenarios; a corollary of this is a finite methane lifetime (45 years at the most). As a result, if methane were to increase significantly enough over a short period, the associated UV-B increase and/or deterioration of surface conditions could provide an explanation for the landmass extinction at the Permian-Triassic boundary.

Citation: Lamarque, J.-F., J. Kiehl, C. Shields, B. A. Boville, and D. E. Kinnison (2006), Modeling the response to changes in tropospheric methane concentration: Application to the Permian-Triassic boundary, *Paleoceanography*, *21*, PA3006, doi:10.1029/2006PA001276.

1. Introduction

[2] The existence of a large $\delta^{13}C$ excursion at the Permian-Triassic boundary 251 Ma [*Krull et al.*, 2000] has been hypothesized to originate from a large release of methane, most likely from the destabilization of continental shelf methane clathrates [*Berner*, 2002; *de Wit et al.*, 2002]. This argument is also used for explaining the $\delta^{13}C$ excursions at the Paleocene-Eocene thermal maximum [*Dickens et al.*, 1995] and in the early Jurassic period [*Kemp et al.*, 2005]. A strong climate response is expected from this methane release, owing to the large methane greenhouse warming potential [*Ramaswamy et al.*, 2001]. In addition, large inputs of methane into the atmosphere can have dramatic effects on its chemistry [*Schmidt and Shindell*, 2003]; this is due to the fact that methane interacts strongly with the hydroxyl radical OH, which is itself the main oxidizing agent in the atmosphere and regulates the lifetime of most reactive species.

[3] In the stratosphere, methane reacts with OH, O^1D, chlorine atoms and, in the upper stratosphere, is photodissociated; all these processes lead to water vapor production [*Coffey and Brasseur*, 1999]. This water vapor is in turn a key component to the destruction of stratospheric ozone. Consequently, a large release of methane can potentially destroy stratospheric ozone [*Schmidt and Shindell*, 2003]; this destruction would lead to an increase in UV-B radiation reaching the surface and potential DNA damage [*Rozema et al.*, 2002]. Recent evidence points to an increase in land plant mutation at the Permian-Triassic boundary, with enhanced UV from decreased ozone a possible explanation [*Visscher et al.*, 2004]. This enhanced UV and/or other chemical impacts from methane release (mostly, increased surface ozone and carbon monoxide and increased surface temperature) could have contributed to the mass extinction at the end of the Permian [*Erwin*, 1994; *Twitchett*, 2006].

[4] The duration of the response to a release of methane is a direct function of its lifetime. Under present-day conditions, the methane lifetime (from its reaction with the hydroxyl radical OH and photodissociation in the stratosphere) is on the order of 10 years [*Stevenson et al.*, 2006]. Because the amount of OH is itself an inverse function of the methane concentration, the methane lifetime is a function of its abundance, with lifetime increasing with increasing methane [*Prather et al.*, 2001].

[5] In a recent study, *Kiehl and Shields* [2005, hereinafter referred to as KS] have used a climate model (forced by a tenfold increase in CO_2 to 3550 parts per million per volume, written hereinafter as ppmv, and realistic biogeography) to simulate many of the observed features of the Permian-Triassic boundary time period on land and in the ocean. We expand this study by looking at the additional role of methane release on climate and atmospheric chemistry at the Permian-Triassic boundary. In particular, we will assess whether, within the plausible range for the amount of methane clathrate release, significant impacts on ozone and methane lifetime will occur. While this study focuses on the Permian-Triassic boundary, many of the conclusions are

[1]National Center for Atmospheric Research, Boulder, Colorado, USA.

0883-8305/06/2006PA001276$12.00

applicable to other time periods affected by large methane releases.

[6] This paper is organized as follows. In section 2, we describe the chemistry-climate model we use to study the impact of methane inputs to the atmosphere. The various methane scenarios, along with their justification, are discussed in section 3. In section 4, we present a brief model evaluation, mostly by comparing our climate results to KS. Section 5 discusses the main results of our simulations. A discussion and conclusions follow in section 6.

2. Model Description

[7] In this study, we use a comprehensive stratospheric/tropospheric atmospheric model with interactive chemistry. This model is similar to the Whole Atmosphere Community Climate Model (WACCM3) [*Sassi et al.*, 2005], except in its vertical extent; indeed, because our main focus is on the troposphere and stratosphere, our model version only extends up to approximately 85 km (as in the Middle Atmosphere Community Climate Model (MACCM) of *Boville* [1995]) with 52 levels. In addition, we have simplified the WACCM3 chemistry due to the absence of man-made compounds. To limit the computer expense of running our model, we have not included a direct representation of nonmethane hydrocarbon chemistry; instead the emissions of these species (mostly isoprene and monoterpenes) are represented as emissions of carbon monoxide (CO), weighted by their CO production yield. Because of the lower carbon monoxide reactivity [*Seinfeld and Pandis*, 1998], this simplification leads to an underestimate of tropospheric ozone, on the order of 10%. Because of this limited bias and because the main sensitivity in this paper is on methane changes, the lack of nonmethane hydrocarbon chemistry does not affect significantly the overall analysis presented in this paper. The list of species and reactions used in our simulations are given in the online supplement, along with a description of the representation of heterogeneous chemistry in polar stratospheric clouds. In the present configuration the model uses a horizontal resolution of 4° (latitude) × 5° (longitude). All physical and chemical processes are calculated using a 30 min time step.

[8] At the surface the atmospheric model uses the land/sea distribution and vegetation cover from KS. In addition, we have included a simplified representation of the ocean using a slab-ocean approach [*Collins et al.*, 2006]. In this approach, the monthly averaged sea surface temperatures (SSTs) from KS are used to define the monthly meridional (latitude-dependent) ocean heat flux necessary to reproduce the simulated SSTs given the other terms affecting the surface temperature budget. Indeed, the surface temperature budget can be summarized by

$$\frac{\partial T_S}{\partial t} = \sum S_F + O_F$$

where T_S is the surface temperature, S_F are the surface fluxes and O_F is the ocean heat flux. Using these equations, the surface temperatures and fluxes from KS are used to calculate O_F. The simulations discussed in this paper then use O_F to calculate the surface temperature using the surface fluxes calculated interactively in the model. Consequently, the SSTs in our model framework are constrained to be equivalent to the SSTs from KS for a similar setup (same methane, CO_2, and solar constant). However, even with this simplified ocean model, the SSTs are able to respond to changes in radiative fluxes from changes in the greenhouse gases. This approach is nevertheless only valid as long as the actual meridional ocean heat fluxes are not significantly affected by those changes.

Table 1. List of Chemical Species With Fixed Lower Boundary Conditions[a]

Chemical Compounds	Surface Mixing Ratio	Comment
N_2O	275 ppbv	preindustrial value
CO_2	3550 ppmv	see KS
CH_3Br	6 pptv	preindustrial value
CH_3Cl	550 pptv	preindustrial value
H_2	250 ppbv	preindustrial value

[a]Preindustrial values are taken from *Gauss et al.* [2006]. Abbreviations are ppbv, parts per billion per volume; ppmv, parts per million per volume; pptv, parts per trillion per volume; and KS, *Kiehl and Shields* [2005].

[9] In the present era, the oxidation in the atmosphere of the biogenic emissions of hydrocarbons by vegetation (such as isoprene and terpenes [*Guenther et al.*, 1995]) represents a significant fraction of the carbon monoxide (CO) global budget. These emissions are species-dependent and display a strong sensitivity to temperature; algorithms representing that dependence (along with a dependence on solar flux) have been recently implemented in the Community Land Model [*Levis et al.*, 2003]. We use this implementation to interactively calculate these biogenic emissions using the Permian vegetation cover as prescribed in KS. Because our representation of the chemistry does not include higher hydrocarbons, these emissions are directly converted to CO with 70% efficiency, the remaining being assumed to be directly converted to CO_2.

[10] Natural emissions of nitrogen oxides (NO_x = NO + NO_2) are from lightning, microbes in the soil and biomass burning from wildfires (which also emit CO). For simplicity and because of the lack of information on wildfires and soils at the Permian/Triassic boundary, we consider only NO_x emissions from lightning. These emissions use the same algorithms [*Price and Rind*, 1994] as in our present-day simulations; these algorithms provide a distribution of lightning emissions that is dependent on the simulated location and strength of convective cloud activity.

[11] In all simulations (see below), we have specified the surface mixing ratio of several chemical species (see Table 1). By specifying the mixing ratio at the surface, we allow the model to transport and chemically process these species above the bottom model layer. In addition, oxygen (O_2) levels are set to 17% [*Berner*, 2002; *Huey and Ward*, 2005].

[12] While it could be expected that sulfur dioxide emissions from volcanoes were present during the simulated period, this was not included in this study.

3. Methane Release Scenarios

[13] As described in section 1, the main purpose of this study is to identify the response of the chemistry and

Table 2. List of Simulations[a]

Simulation Name	Methane Surface Mixing Ratio, ppmv	Duration, years	Comment
1x	0.700	30	continuation of KS, base scenario
10x	7	30	
100x	70	30	
250x	175	10	
750x	525	10	
1000x	700	30	
2500x	1750	10	
5000x	3500	10	
10000x	7000	4	unstable simulation
Reduced NO	70	10	lightning emissions are divided by 2
Reduced CO	70	10	CO surface emissions are set to 0
Reduced H_2O	70	10	water vapor seen by the chemistry is divided by 1.5

[a]Methane surface mixing ratio is expressed in parts per million per volume (ppmv).

climate to methane release. Because simulations with our model are quite expensive, we cannot perform transient experiments such as the studies by *Schmidt and Shindell* [2003] or *Kump et al.* [2005]. Therefore we have chosen to specify the methane mixing ratio at the surface in order to reflect changes in emissions. The use of a constant methane surface concentration is in essence representative of the following scenario: a large burst of methane is released into the atmosphere and brings instantaneously the methane concentration to the desired level. This is formally followed by a (much smaller) continuous influx sufficient to sustain this level as methane is transported out of the surface layer and is chemically destroyed. If we consider the estimated Permian-Triassic boundary methane clathrate release of 4200 Gt (C) [*Berner*, 2002], this amount could translate to a 2700-fold increase of the methane surface mixing ratio compared to its preindustrial value (approx. 0.7 ppmv, valid for 1850). This 2700-fold increase is in many respects an upper bound on the methane response; indeed it assumes that (1) all the methane released at the bottom of the ocean reaches the atmosphere and (2) that the release is instantaneous. A key unknown in this scenario is clearly the speed at which the methane is released. While it has recently been argued that the release was very rapid (<2 kyr [*Kemp et al.*, 2005]), this is still very uncertain.

[14] Under this scenario, we have defined a set of simulations (see Table 2) that span a range of methane surface concentration from 0.7 ppmv (hereinafter referred to as 1x; this is our reference case as it corresponds to no methane clathrate release) to 3500 ppmv (5000x). While many simulations were for 30 years (to ensure a fully stabilized climate over the whole model domain), several simulations were 10 years long only as this simulation length was found to be sufficient for the chemistry to be equilibrated. These shorter simulations were performed to provide a more complete view of the chemistry-climate response to methane changes or to perform sensitivity studies. All simulations were initialized (for chemistry and climate variables) from the results of a 20-year 1x simulation.

4. Model Evaluation

[15] In this section, we evaluate the most relevant features of the 1x simulation. As this simulation is similar in its setup to and a continuation of KS (in which the atmospheric model extends up to 40 km instead of 85 km and has no interactive chemistry), we first compare our simulation of the Permian climate to theirs. This comparison focuses on the following three main climate indicators: surface temperature, zonal average temperature, and zonal wind. The surface temperature (Figure 1) indicates that the annual surface temperature has the same overall distribution, with high tropical temperatures (above 305 K). The largest differences are on the order of 4°–6° (in absolute value) and located over land; these differences arise from differences in the regional distribution of precipitation between the two models. In the zonal mean, the differences in temperature (Figure 2) are largest in the stratosphere, where the interactive ozone distribution in our 1x simulation is slightly different from the climatology used in KS, which is valid for present-day conditions. Similarly, the zonal mean zonal wind (Figure 3) distributions are very similar in the two models, with the differences smaller than the natural variability. These and other diagnostics (e.g., the annual global precipitations, cloud cover and radiative surface fluxes) indicate that the simulated climate is similar enough to the results of KS to qualify them as equivalent.

[16] With respect to chemistry, there are no data or other simulations we can compare to our results. On the other hand, we have used the same model for preindustrial and present-day calculations [*Gauss et al.*, 2006]. The simulated (Permian and present-day) zonal mean annual average ozone mixing ratio is therefore shown (Figure 4) along with a satellite-based climatology [*Randel et al.*, 1998]. The present-day calculation shows a slight overestimate of the ozone maximum in the tropical regions but, on an annual basis, many of the observed features are well reproduced by the model. This present-day simulation gives us the indication that the model compares reasonably well with available climatologies. It is interesting to note that the maximum ozone values are larger and located at higher altitude in the Permian simulation. A possible explanation for this pattern is the colder stratosphere (by 15–20 K) in the Permian compared to present-day conditions (not shown); this cooling is due to the larger CO_2 concentration in the stratosphere [*Brasseur and Solomon*, 1986].

5. Results

[17] This section describes some of the model response to the imposed changes in methane. Our analysis focuses on

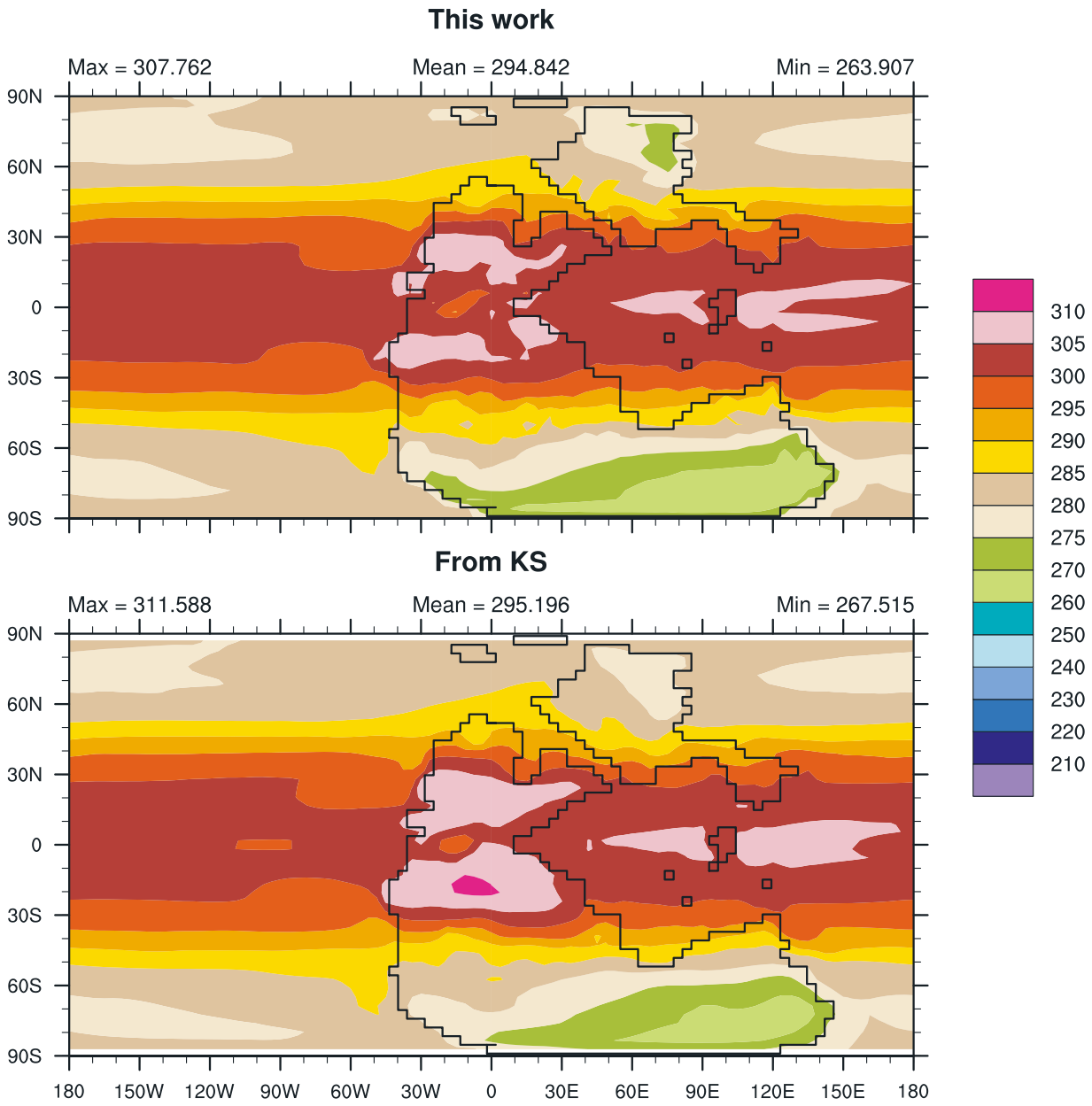

Figure 1. Simulation of the annual averaged surface temperature (in K) from KS and this work.

(1) ozone, (2) the hydroxyl radical OH and (3) surface living conditions.

5.1. Ozone

[18] In response to increased methane the total ozone column (i.e., the mass-weighted integral of the ozone mixing ratio from the surface to the model top; Figure 5, rightmost top panel) increases slightly up to the 250x methane level. Above those levels, the total ozone column rapidly collapses. The 10000x simulation (not shown) indicates that this ozone collapse actually accelerates; this simulation was unfortunately of 4 years duration because of model limitations for near-zero stratospheric ozone levels. However, it is likely that such extreme levels of methane will be associated with phenomena (such as methane haze) that are not adequately or at all simulated by this model and make this simulation hard to interpret.

[19] Our ozone response is in contrast with the similar study (albeit for the Paleocene/Eocene Thermal Maximum) by *Schmidt and Shindell* [2003]. Indeed our total (tropospheric and stratospheric, and also the column above 200 hPa as given by *Schmidt and Shindell* [2003], not shown) ozone column is extremely resilient to changes in methane, up to an increase of 750 times its preindustrial level; we hypothesize that this discrepancy is related to their use of a simplified linear stratospheric chemistry, in which large nonlinear deviations from the undisturbed case can be misrepresented.

[20] The ozone response to methane changes is a combination of lower and upper atmosphere changes. To illustrate

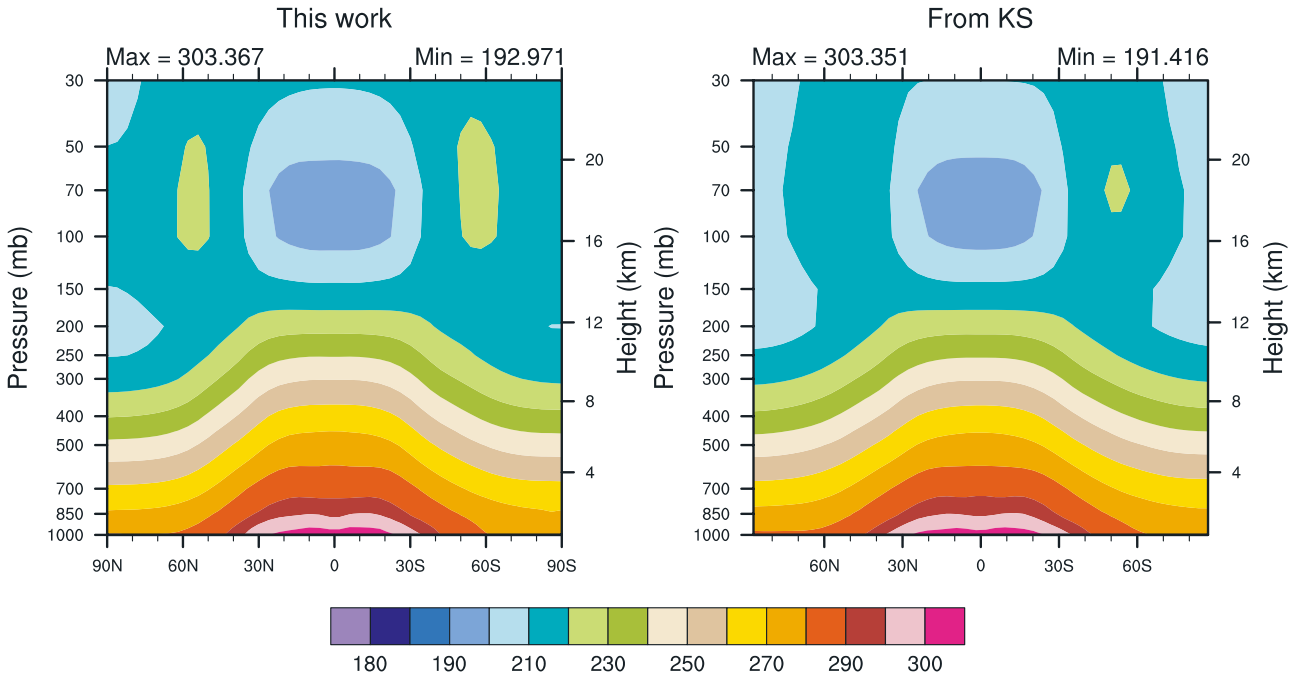

Figure 2. Simulation of the annual zonally averaged temperature (in K) from KS and this work.

that point, we show in Figure 6 the zonal mean difference in ozone mixing ratio between each simulation and 1x. In the upper stratosphere, the ozone exhibits a continuous decline. Indeed, in the region around 50 km (1 hPa), the ozone lifetime is very short [*Brasseur and Solomon*, 1986] and a steady state equation shows the main factors influencing the ozone mixing ratio in that region [*Allen et al.*, 1984] is

$$[O_3] \propto \frac{J_2^{2/3}}{\left(J_4^{2/3} J_3^{1/3} [H_2O]^{1/3}\right)} \quad (1)$$

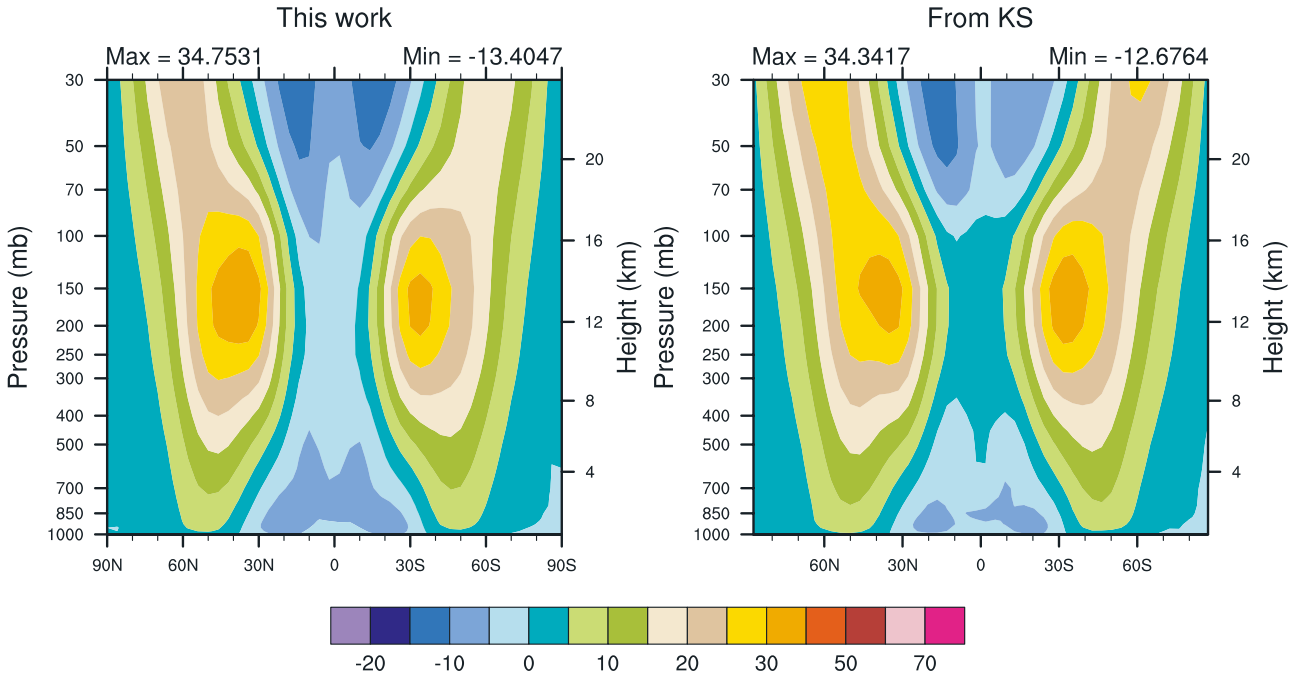

Figure 3. Simulation of the annual zonally averaged zonal wind (in m/s) from KS and this work.

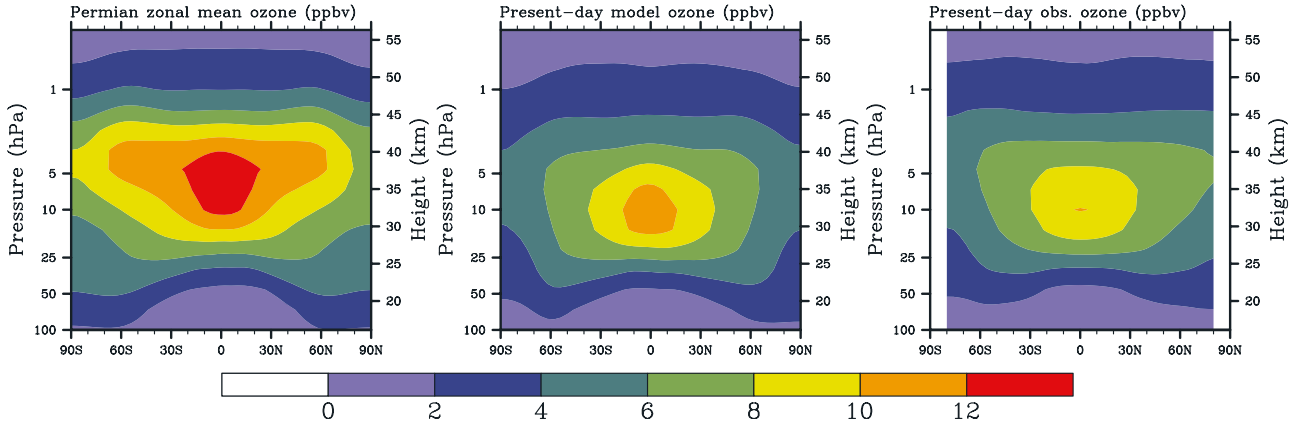

Figure 4. Comparison of the annual zonally averaged ozone mixing ratio (in ppmv) for (left) the 1x simulation, (middle) a present-day simulation with the same model framework [see *Gauss et al.*, 2006], and (right) a satellite-based climatology (data are from *Randel et al.* [1998]).

where the Js are the photolysis rate of oxygen and ozone, respectively; the numbering of the Js is according to the list of photolytic reactions in Table S3 in the auxiliary material[1]. In this equation the proportionality coefficient is dependent on quantities (temperature, nitrogen and oxygen) that will vary little between simulations. In Figure 7, we indeed show the almost linear relationship between the simulated ozone (left-hand side of equation (1)) and the right-hand side of equation (1). We see that all simulations display the same relation; consequently the above formula is an appropriate description of the ozone in the upper stratosphere in all cases. Therefore, in that region, equation (1) shows that the ozone decrease is in direct response to the increased water vapor from increasing methane. Above this region, the

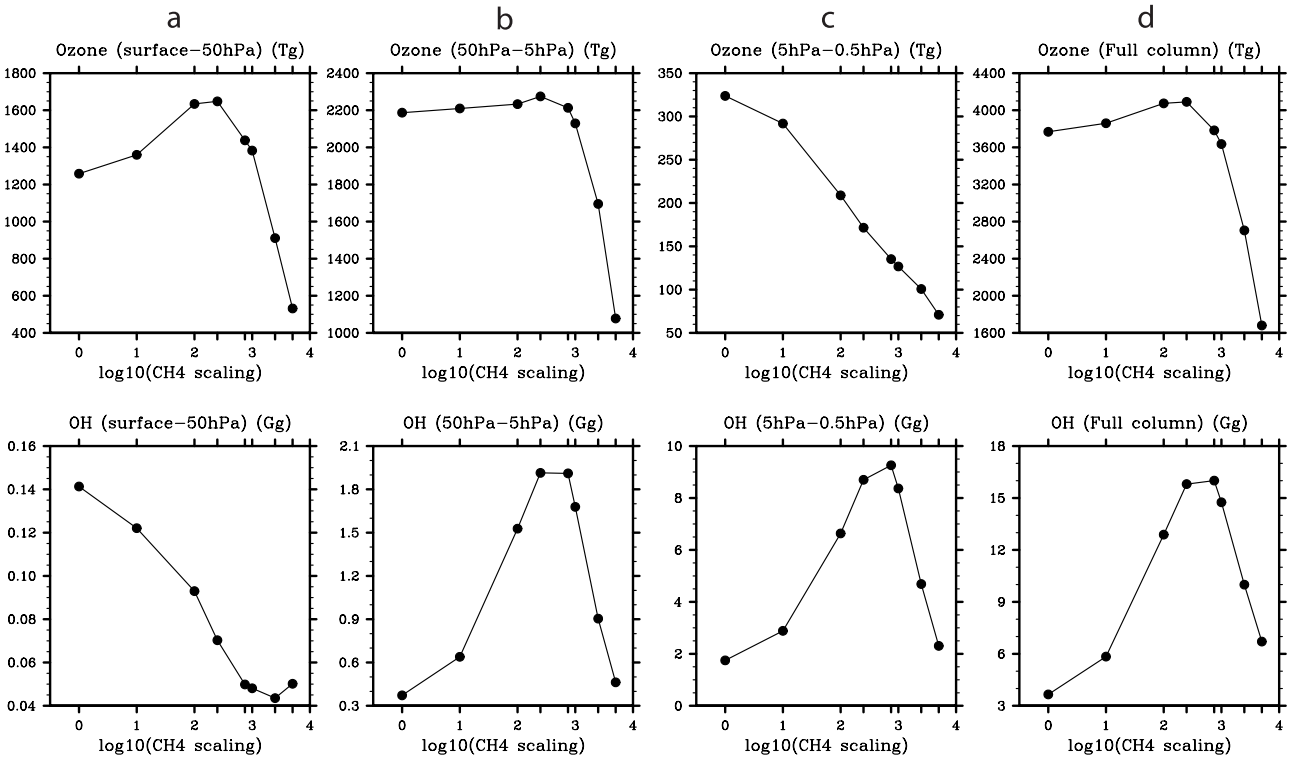

Figure 5. Global integral of the mass-weighted integrated column (in Tg) of (top) ozone (10 Tg ≈ 1 Dobson Unit) and (bottom) the hydroxyl radical (OH). Integrals from the (a) surface to 50 hPa (20 km, approximately the tropopause height in the tropics), (b) 50 hPa to 5 hPa (40 km), and (c) 5 hPa to 0.5 hPa (55 km). (d) Total column. In Figures 5a–5d the horizontal axis is the logarithm of the increase in methane over the 1x simulation (see Table 2).

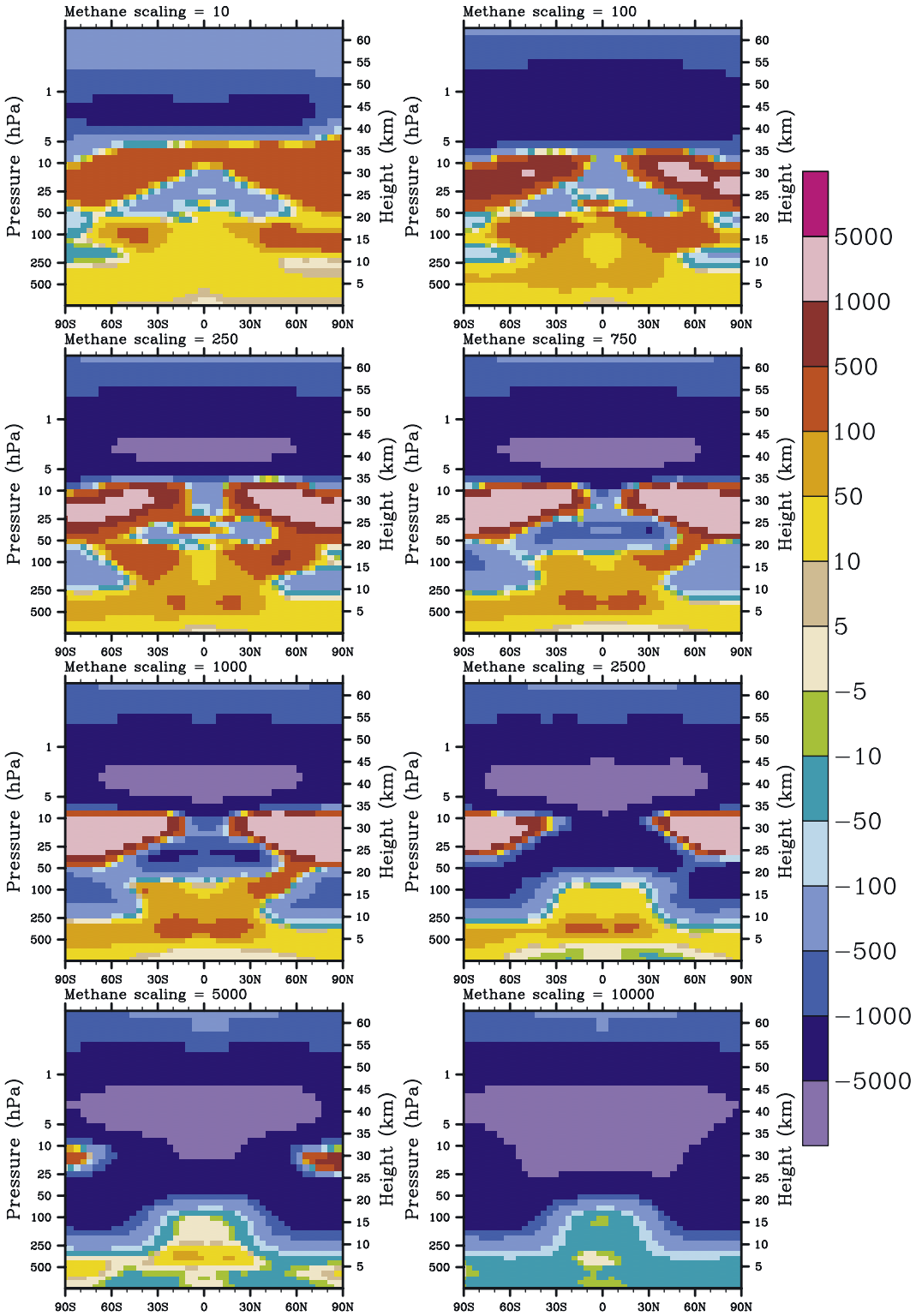

Figure 6. Difference in annual zonally averaged ozone mixing ratio (ppbv) between each simulation (see Table 2) and the 1x simulation. (top left) The 10x simulation. (top right) The 100x simulation. All other panels follow the order in methane increases (see Table 2).

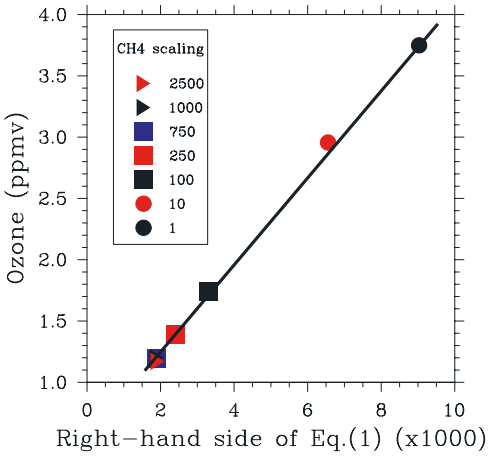

Figure 7. Correlation between the simulated ozone and equation (1). Each symbol corresponds to a specific simulation (see legend). A linear fit indicates that equation (1) is an accurate description of the main parameters responsible for the ozone distribution in the tropical regions at 50 km.

exponent to H_2O in the denominator becomes $^1/_2$ at 70 km and 1 at 80 km [*Allen et al.*, 1984]. In conclusion, this analysis shows that, at all altitudes above 50 km, the ozone rapidly decreases with increasing methane and associated water vapor.

[21] Below this region but above 20 km (50 hPa, see Figure 5) there is actually an increase in ozone in the extratropics, up to the 2500x simulation. This is due to the fact that the disappearing ozone column above increases the ozone production below from the stronger O_2 photolysis, which is the main ozone production channel in the stratosphere. This self-healing effect is critical in enabling the total ozone column to stay relatively constant (less than a 10% variation) while increasing methane concentrations by almost 3 orders of magnitude, from the 1x to the 750x case. Above that threshold however, the self-healing feedback stops being effective enough as the ozone loss increases faster than the increased productivity and the ozone column collapses.

[22] In the lower stratosphere (between 30 and 100 hPa) a significant fraction (approximately 10% in the 5000x case, not shown) of the ozone loss is associated with the increase of optically thin clouds in the lower stratosphere/upper troposphere (Figure 8). Indeed, the increase of water in that part of the atmosphere (from increased methane photooxidation and increase in the temperature at which tropospheric air enters the stratosphere in the tropical regions, which allows higher water vapor mixing ratio to penetrate the tropical stratosphere), compounded with a significant drop in stratospheric temperature (as the atmosphere loses the radiative heating from ozone absorption, Figure 9), leads to an increase in surface area available for heterogeneous chemistry and ozone loss, similar to the present-day ozone loss in the polar regions; however, since the chlorine levels are quite low under the chosen Permian conditions (Table 1), this heterogeneous loss represents only a fraction of the ozone loss. The bulk of the ozone loss is associated with a large increase in HO_2, a direct impact of the increased amount of water in the stratosphere. This increase in HO_2 leads to a decrease in ozone through reactions 47 and 48 of Table S2 in the auxiliary material.

[23] Regarding the rise of ozone in the simulations up to 250x (Figure 5), we see that most of it is concentrated in the lower part of the atmosphere (between the surface and 50 hPa). With increasing methane, increasing tropospheric amounts of CO (from methane oxidation and temperature-dependent biogenic emissions) and NO_x (from convection-triggered lightning) are found (not shown) in association with the warmer (and hence more convective) climate so that increased ozone production ensues. Indeed, in the presence of OH and NO_x, CO leads to the production of ozone via the following chemical pathway (of several possible pathways for ozone production by hydrocarbon oxidation)

$$\begin{aligned} OH + CO &\rightarrow CO_2 + H \\ H + O_2 + M &\rightarrow HO_2 + M \\ HO_2 + NO &\rightarrow NO_2 + OH \\ NO_2 + h\nu &\rightarrow NO + O \\ O + O_2 + M &\rightarrow O_3 + M \end{aligned}$$

where M indicates a three-body reaction and $h\nu$ indicates photolysis. However, beyond the 250x simulation, the ozone mixing ratio decreases from the presence of very high HO_2 concentrations, as can be seen from the negative values close to the surface in Figure 6. This decrease, compounded by the large stratospheric decrease, leads to the ozone column collapse shown in Figure 5.

5.2. Hydroxyl Radical OH

[24] While OH is the main sink of methane, there is no level of methane for which the OH completely disappears (Figure 5). This seems counterintuitive as the levels of methane simulated in this study are so large that it could be expected that it would virtually eliminate OH, which by itself leads to interesting air quality issues [*Lelieveld et al.*, 2004]. However, the increase in water vapor in the atmosphere leads to an increased production of OH (from $O(^1D) + H_2O$, reaction 6 in Table S2 in the auxiliary material, with $O(^1D)$ coming from the photolysis of ozone); a sensitivity analysis for the 100x case actually shows that this water vapor feedback is equivalent in magnitude to the tropospheric OH loss from increased methane. The persistence of a low but significant amount of tropospheric OH is crucial in keeping the methane lifetime (whose value is dictated by the reaction of methane with OH and the photooxidation of methane in the stratosphere) bounded. In our simulations, the methane lifetime never exceeds 45 years (Figure 10), similar to *Schmidt and Shindell* [2003]. This in turn has the implication that, however large the methane perturbation is, this perturbation will never last more than a few centuries. In addition, in the 5000x case, the tropospheric OH is actually larger than in the 2500x case. This "rebounding"

[1] Auxiliary material data sets are available at ftp://ftp.agu.org/apend/PA/2006PA001276. Other auxiliary material files are in the HTML.

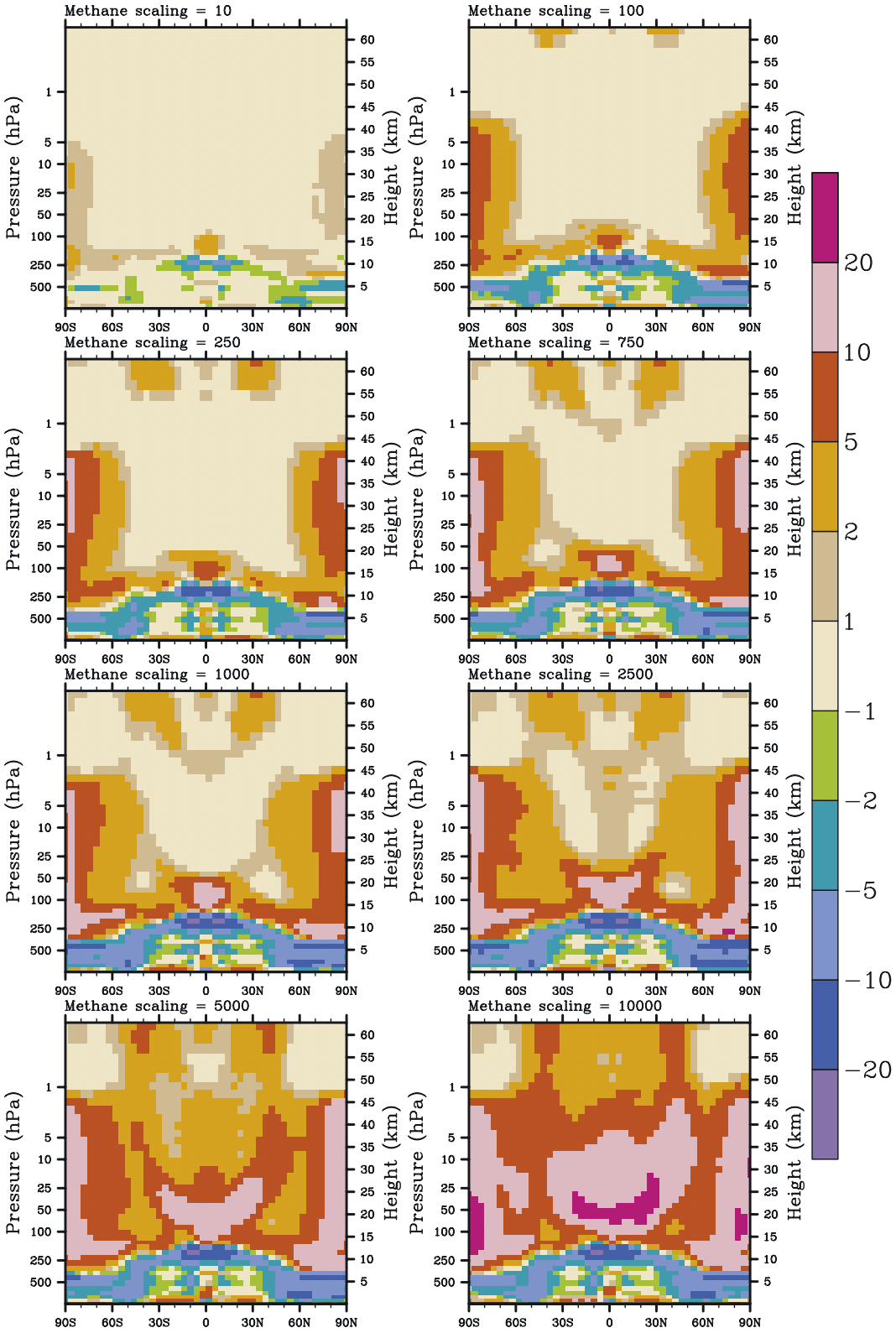

Figure 8. Difference in annual zonally averaged cloud fraction (in percent) between each simulation (see Table 2) and the 1x simulation. (top left) The 10x simulation (top right) The 100x simulation. All other panels follow the order in methane increases (see Table 2).

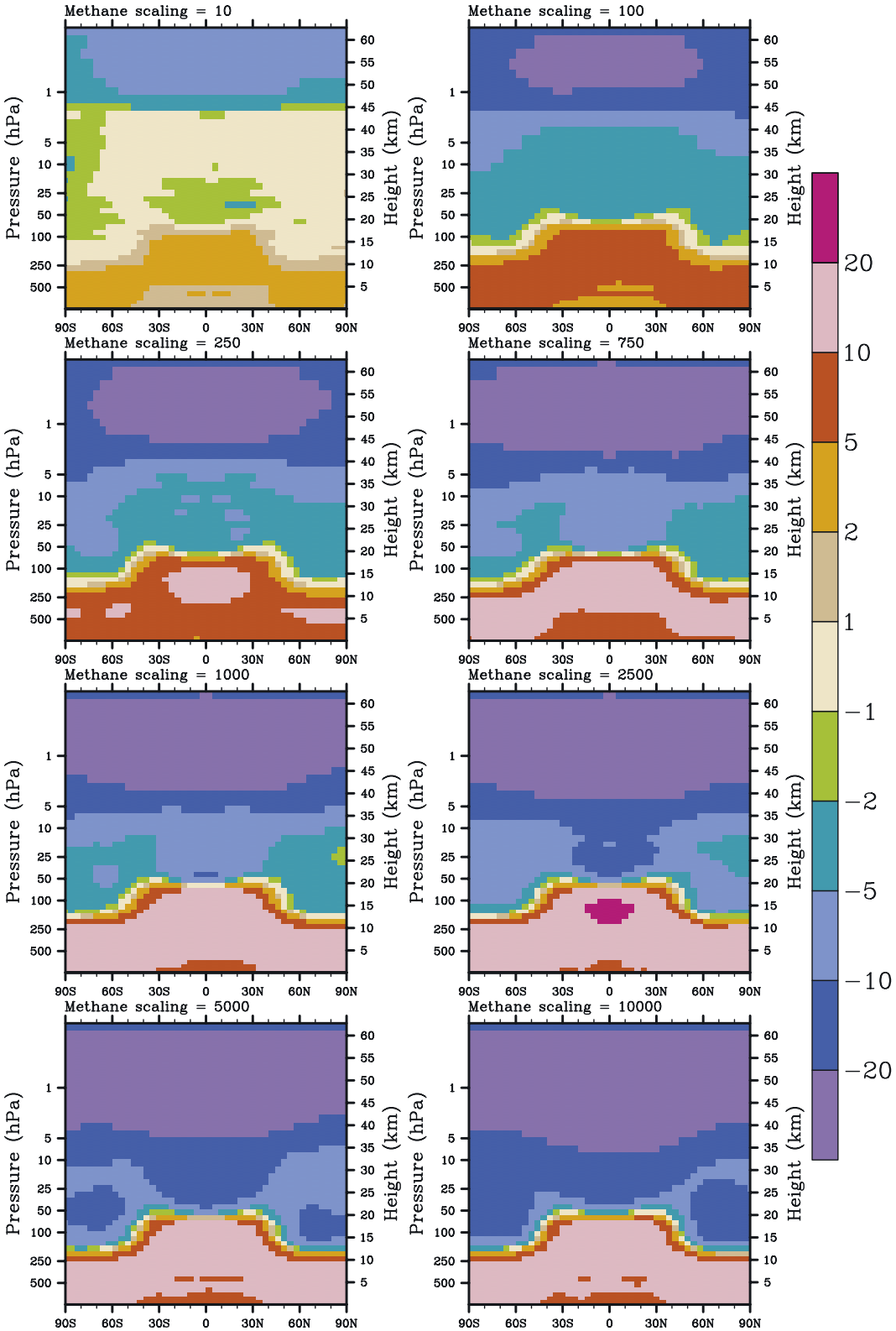

Figure 9. Same as Figure 8 but for temperature.

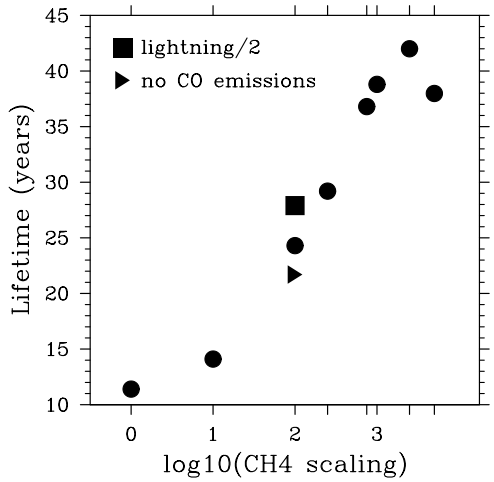

Figure 10. Estimated methane lifetime (in years). The horizontal axis is the logarithm of the increase in methane over the 1x simulation (see Table 2). The circles are for the standard simulations; the square and triangle are for the sensitivity experiments with respect to NO_x and CO emissions, respectively (see Table 2 for details).

is associated with the collapse of stratospheric ozone which increases the photolysis rates in the troposphere and hence the OH production [*Granier and Shine*, 1998]. This behavior (which is further amplified in the 10000x simulation, not shown) could enable an ozone recovery in the stratosphere by increasing the removal rate of methane. This will be studied in more detail in a subsequent paper.

[25] The existence of significant OH concentrations at all methane levels studied is related to the chemical state of the atmosphere, which in turn depends strongly on the emissions of chemically active gases. As described in section 2, there is large uncertainty associated with the amplitude of the hydrocarbon biogenic emissions and the lightning NO_x emissions. Therefore, to test the sensitivity of our overall results to these emissions, we have performed two additional 100x simulations in which each of these emissions are artificially altered (see Table 2). When the CO surface emissions are eliminated (identified by the triangle in Figure 10), the lifetime of methane decreases by approximately 2.5 years as the tropospheric OH burden is increased by about 35%; indeed the oxidation of CO by OH is the largest OH sink in the troposphere and a reduction in CO emissions directly translates in an increase of OH. On the other hand, the reduction of NO_x emissions from 12 Tg (N) per year to 6 (identified by the square in Figure 10) tends to decrease the tropospheric OH burden by approximately 30% and increase the methane lifetime by over 3 years. This is because NO_x emissions are central to the formation of ozone (which is photodissociated and reacts with water vapor to create OH) in the troposphere; the assigned decrease in lightning NO_x emissions reduces the tropospheric OH burden by 20%. Therefore these sensitivity experiments indicate that, while there is a large uncertainty in surface emissions, this uncertainty has only a limited impact on the overall behavior of the simulated system.

5.3. Surface Air Quality

[26] Surface temperature and relative humidity increase in response to increase in methane, a direct consequence of the strong greenhouse gas effect of methane. In particular, the globally averaged surface temperature in the 1000x simulation has increased an additional 10°C over the KS results (Figure 11). In addition, the moisture content of the troposphere (measured here by the integrated precipitable water) has more than doubled between the 1x and 1000x cases. The combination of these factors is used to define the surface heat index HI (see http://www.srh.noaa.gov/ffc/html/studies/ta_htindx.PDF)

$$\begin{aligned} HI = &-42.379 + 2.04901523T + 10.1433127R \\ &- 0.22475541TR - 6.83783 \times 10^{-3}T^2 \\ &- 5.481717 \times 10^{-2}R^2 + 1.22874 \times 10^{-3}T^2R \\ &+ 8.5282 \times 10^{-4}TR^2 - 1.99 \times 10^{-6}T^2R^2 \end{aligned} \quad (2)$$

which is designed for humans and represents the temperature the body feels when heat and humidity are combined. Temperatures above 54°C are considered extremely dangerous. With increasing methane (Figure 12) the heat index reaches very large values over a significant portion of the continental masses, especially in the tropical regions. The degradation of the living conditions in the tropics is in qualitative agreement with the land plant evolution across the Permian-Triassic boundary described by *Rees* [2002]; in that study, it was indeed shown that the largest number of plant genera after the Permian-Triassic extinction occurred at high latitudes.

[27] In addition to deteriorating climate conditions, increasing methane levels are associated with increasing carbon monoxide and ozone levels (Figures 13 and 14, respectively). It has been estimated that carbon monoxide levels of 1000 ppmv are required to be instantly deadly to humans; however, it is unclear how that would translate to other organisms. In our simulations, the surface carbon monoxide levels never reach annual averages larger than

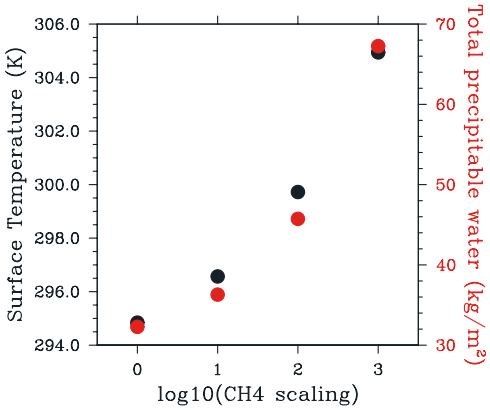

Figure 11. Global and annual average of surface temperature (in K) (black circles, left axis) and total precipitable water (in kg/m^2) (red circles, right axis).

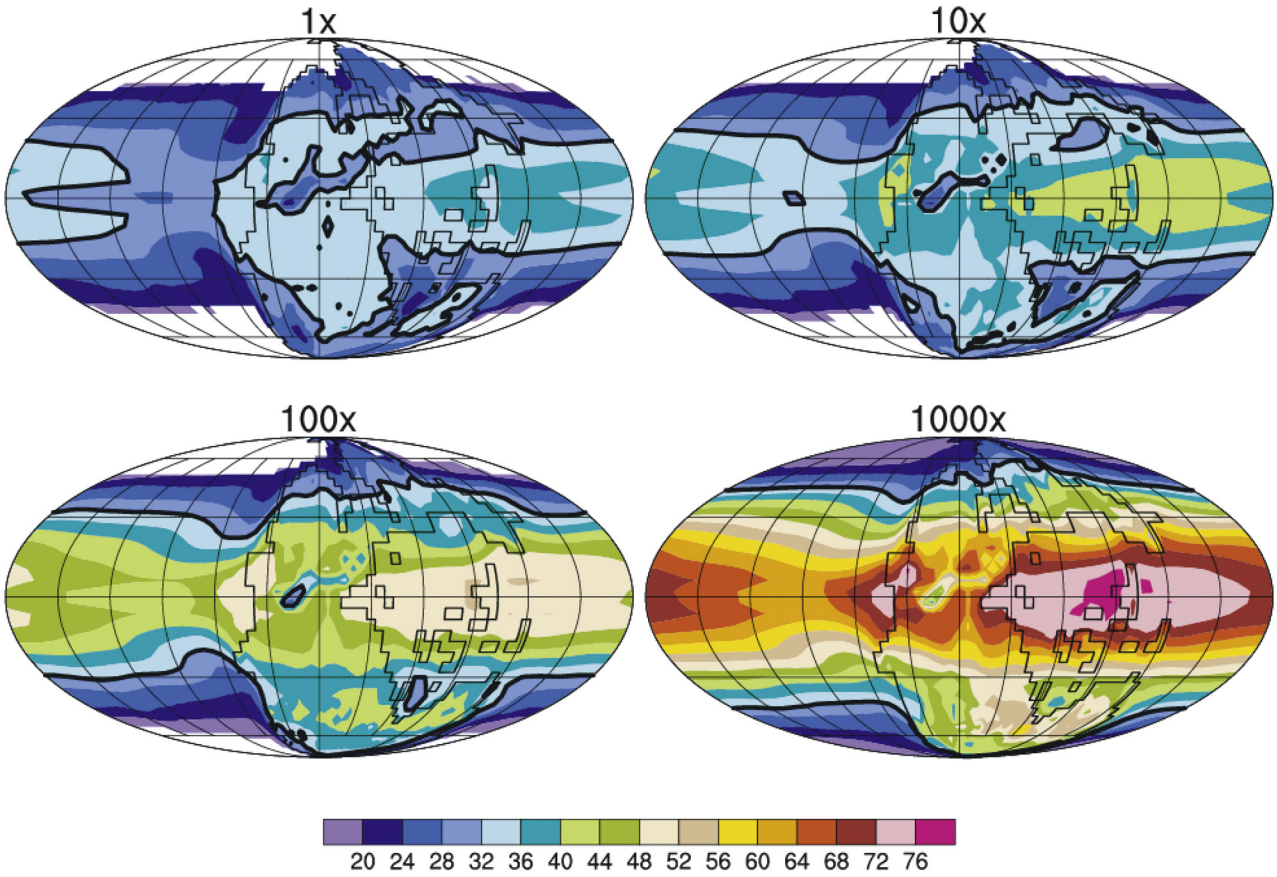

Figure 12. Annual average of the heat index (see equation (2)) at the surface for the (top left) 1x, (top right) 10x, (bottom left) 100x, and (bottom right) 1000x simulations. The solid black line indicates the 32°C threshold.

17 ppmv, far lower than the aforementioned critical level. With respect to ozone, surface levels are 100 ppbv or less, also well below critical levels. In both cases, the largest concentrations are found at the highest latitudes, in contrast to the climatic impact of increased methane. If the flora and fauna of the Permian had a similar tolerance to ozone and CO as humans, then it is unlikely that chemical toxicity by those compounds was responsible for the extinction at the Permian/Triassic boundary.

[28] Associated with the decrease in total ozone for the simulations 750x and beyond, we find that surface UV-B (calculated as the solar flux at 300 nm reaching the surface) has increased by a factor of 7 in the 5000x case (Figure 15); this increase in UV-B radiation directly translates into DNA damage [*Rozema et al.*, 2002]. Therefore, if such increase in UV-B were to occur, this could have a significant impact on the survival rate of plants and animals and on their adaptive mutations.

6. Discussion and Conclusions

[29] In this study, we have modeled the response of the chemistry-climate system to changes in methane loading at the Permian-Triassic boundary; the amplitude of those changes is commensurate with the hypothesized release of methane clathrates from marine shelves [*Berner*, 2002].

[30] We find that the total (tropospheric and stratospheric) ozone column is extremely resilient to changes in methane, up to an increase of 750 times its preindustrial level. This resilience is achieved through equilibrium between losses in the upper stratosphere (from increased water vapor) and a self-healing effect below. Beyond this, further increases in methane eventually lead to the collapse of ozone. However, at extremely large methane concentrations (>5000 times its preindustrial level), there is indication that the steady state tropospheric OH stops decreasing and is actually larger than for lower methane concentrations; this additional OH induces a chemical sink that will increase the removal rate of the accumulated methane, possibly providing a positive feedback for ozone recovery.

[31] Under the highest methane loading simulated (5000 times preindustrial), the ozone column decreases by more than 50% on a global and annual average. This indicates that UV-B levels at the surface will increase sevenfold under that scenario. If adaptation to UV changes can be detected and quantified in paleoproxies, then this might provide insight into the behavior of the ozone column for that period. Note, however, that the UV-B radiation rate of

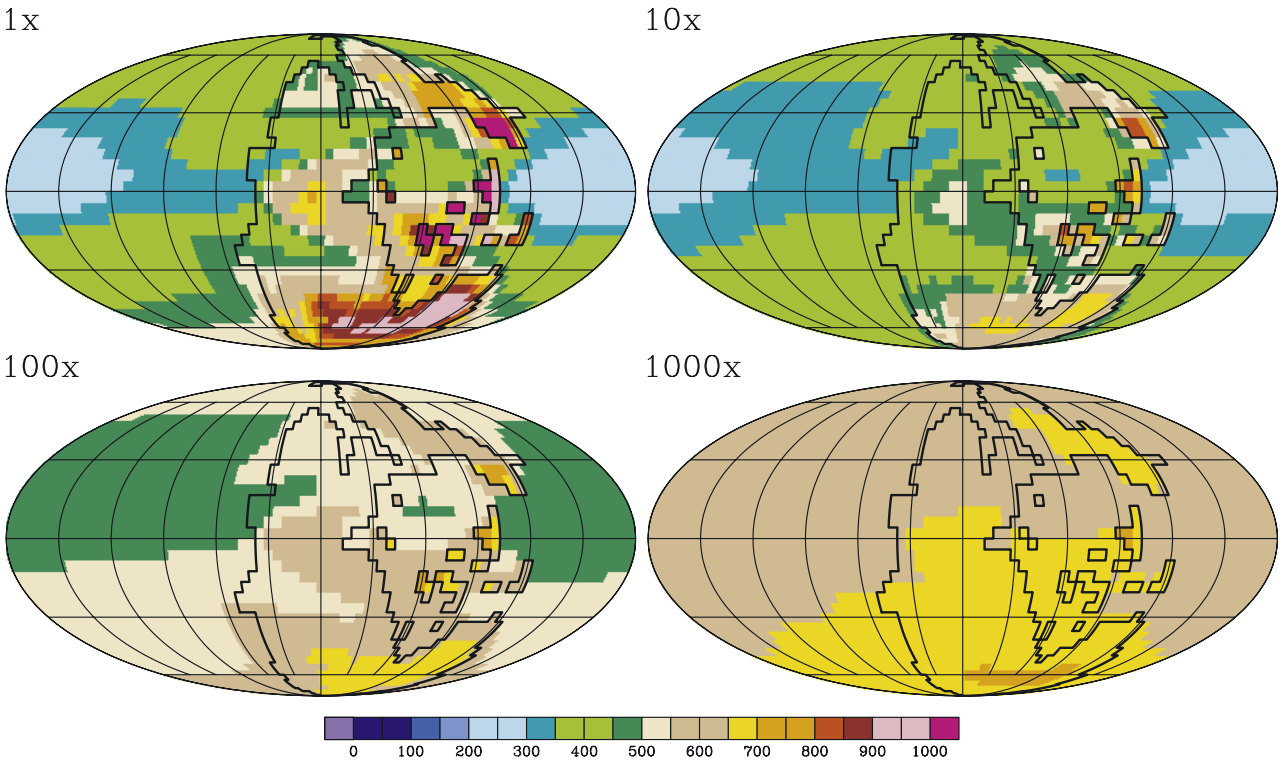

Figure 13. Annual average of the surface carbon monoxide mixing ratio (in ppmv). The (top right) 10x values are divided by 2, (bottom left) 100x values are divided by 5, and (bottom right) 1000x values are divided by 25.

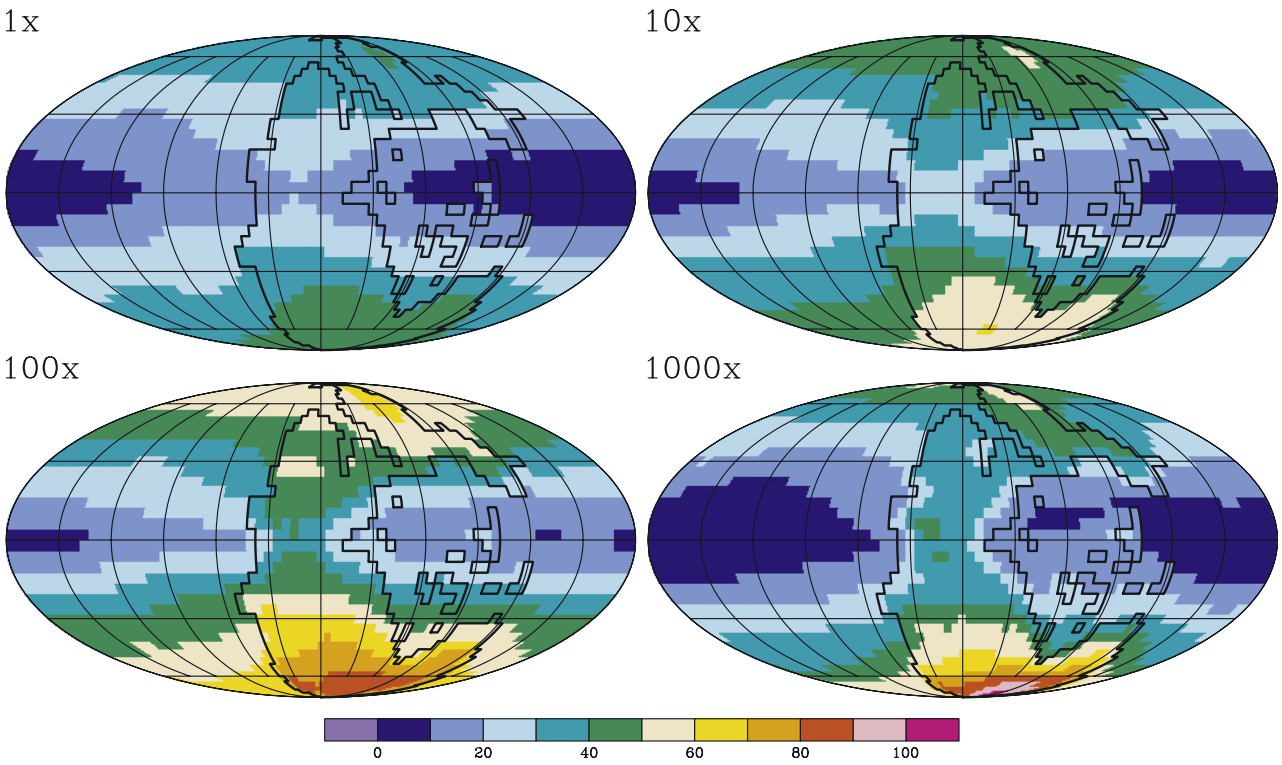

Figure 14. Annual average of the surface ozone mixing ratio (in ppmv).

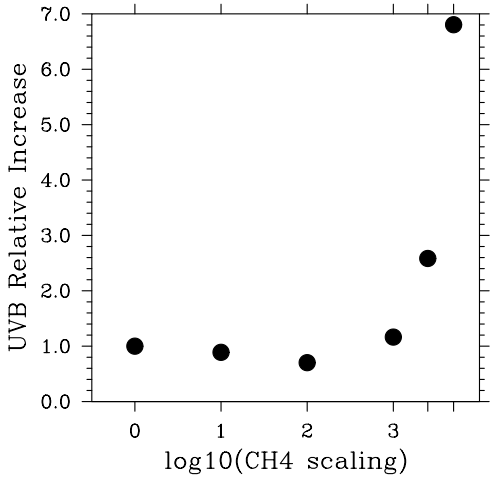

Figure 15. Relative increase in UV-B radiation (at 300 nm) at the surface for a variety of surface methane scenarios. The horizontal axis is the logarithm (base 10) of the methane increase over the 1x case (see Table 2).

increase is very rapid once the ozone column starts collapsing (Figure 15), making the reverse connection (UV damage to ozone) highly sensitive to the accuracy level of the UV impact.

[32] In addition, living conditions at the surface deteriorate considerably under large methane concentrations. This is achieved mostly through the result of an increase in surface temperature and humidity (exemplified here by the heat index) and, to a much smaller extent, an increase in CO and ozone concentrations. However, there is no indication that the latter reach levels high enough to become lethal. To our knowledge, there are no data available at this point to discriminate between the global (UV-B increase) or the land-only (living conditions) hypothesis.

[33] Under no methane scenarios does the OH ever disappear. A corollary to this result is the finite lifetime (actually < 50 years) of methane. This has the important implication that methane perturbations are short-lived, no matter how large they are.

[34] The increase in methane and decrease in stratospheric ozone has the direct consequence of warming the lower atmosphere and cooling the upper atmosphere. Indeed, the disappearance of most of the stratospheric ozone and the warming of the troposphere leads to an elevation of the tropopause; in the tropical regions, the tropopause rises from approximately 18 km in the 1x case to 22 km in the 5000x case (Figure 16). On the other hand, in the stratosphere, the temperature maximum around 50 km has almost completely disappeared in the 5000x case, a consequence of the lack of ozone absorption in that region. In addition, the increased methane leads to a moistening of the atmosphere. This moistening is not restricted to the troposphere but extends to the stratosphere as well, where the photooxidation of methane produces water vapor. With increasing methane, we have indeed found an increase in the prevalence of polar stratospheric clouds in both hemispheres. However, the analysis of their optical thickness (not shown) indicates that these clouds contribute little to the radiative balance of the polar regions, owing to their small water content. It is therefore unlikely that these clouds could play a significant role in amplifying the increase of surface temperature over these regions, as hypothesized by *Sloan and Pollard* [1998].

[35] Our study shows that, if tropospheric methane were to increase to 1750 ppmv (2500 times preindustrial conditions) or more, the associated UV-B increase (from atmospheric ozone collapse) and/or deterioration of surface conditions could provide an explanation for the landmass extinction at the Permian-Triassic boundary. While the amount of methane needed to provoke an ozone collapse is very high and possibly higher than the estimates of the total methane clathrate release at the Permian-Triassic boundary [*Berner*, 2002], the tropospheric OH sink from large hydrogen sulfide emissions [*Kump et al.*, 2005; J.-F. Lamarque et al., The role of hydrogen sulfide in a Permian-Triassic boundary ozone collapse, submitted to *Geology*, 2006) can significantly lower the methane emissions needed to reach a tropospheric concentration that will lead to an ozone collapse. The combination of hydrogen sulfide and methane would make an ozone collapse much more likely than methane alone.

[36] Finally, we have shown that the overall response of ozone is a combination of gas-phase chemistry, heterogeneous chemistry and dynamics (there is some evidence that our simulated stratospheric circulation has accelerated under our increased methane scenarios, not shown) which cannot be easily captured by simplified models. While it is clear that some features in our model will need to be revised or expanded, and others will need to be included in order to explore the full range of possible conditions, studies with fully coupled chemistry-climate models are shedding some new light on the important problem of the response of the climate and atmospheric composition to extreme events.

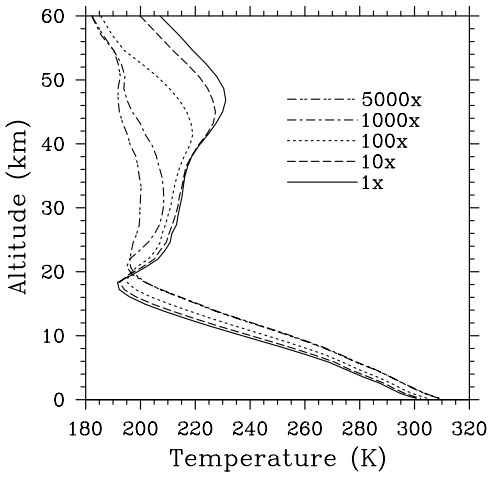

Figure 16. Vertical distribution of the annual and zonally averaged temperature at the equator for a variety of surface methane scenarios. Note the cooling in the stratosphere and the rise in the tropopause height.

[37] **Acknowledgments.** We would like to thank F. Sassi for his help with the model development and S. Madronich for stimulating discussions. R. Garcia and J. Orlando provided comments that greatly improved an earlier version of this manuscript. In addition, we would like to acknowledge the two anonymous reviewers who provided insightful and constructive suggestions. J.F.L. was supported by the SciDAC project from the Department of Energy. This research used resources of the National Energy Research Scientific Computing Center, which is supported by the Office of Science of the U.S. Department of Energy under contract DE-AC03-76SF00098. The National Center for Atmospheric Research is operated by the University Corporation for Atmospheric Research under sponsorship of the National Science Foundation.

References

Allen, M., J. I. Lunine, and Y. L. Yung (1984), The vertical distribution of ozone in the mesosphere and lower thermosphere, *J. Geophys. Res.*, *89*, 4841–4872.

Berner, R. A. (2002), Examination of hypotheses for the Permo-Triassic boundary extinction by carbon cycle modeling, *Proc. Natl. Acad. Sci. U. S. A.*, *99*, 4172–4177.

Boville, B. A. (1995), Middle atmosphere version of CCM2 (MACCM2): Annual cycle and interannual variability, *J. Geophys. Res.*, *100*, 9017–9040.

Brasseur, G. P., and S. Solomon (1986), *Aeronomy of the Middle Atmosphere*, 2nd ed., Springer, New York.

Coffey, M., and G. P. Brasseur (1999), Middle atmospheric ozone, in *Atmospheric Chemistry and Global Change*, edited by G. P. Brasseur, J. J. Orlando, and G. S. Tyndall, pp. 487–513, Oxford Univ. Press, New York.

Collins, W. D., et al. (2006), The formulation and atmospheric simulation of the Community Atmosphere Model: CAM3, *J. Clim.*, *19*, 2122–2143.

De Wit, M. J., et al. (2002), Multiple organic carbon isotope reversals across the Permian-Triassic boundary of terrestrial Gondwana sequences: Clues to extinction patterns and delayed ecosystem recovery, *J. Geol.*, *110*, 227–240.

Dickens, G. R., et al. (1995), Dissociation of oceanic methane hydrate as a cause of the carbon isotope excursion at the end of the Paleocene, *Paleoceanography*, *10*, 965–971.

Erwin, D. H. (1994), The Permo-Triassic extinction, *Nature*, *367*, 231–236.

Gauss, M., et al. (2006), Radiative forcing since preindustrial times due to ozone change in the troposphere and the lower stratosphere, *Atmos. Chem. Phys.*, *6*, 575–599.

Granier, C., and K. P. Shine (1998), Climate effects of ozone and halocarbon changes, in *Scientific Assessment of Ozone Depletion: 1998*, *Global Ozone Res. Monit. Proj.Rep. 44*, vol. 2, chap. 10, pp. 10.1–10.37, World Meteorol. Organ., Geneva, Switzerland.

Guenther, A., et al. (1995), A global model of natural volatile organic compound emissions, *J. Geophys. Res.*, *100*, 8873–8892.

Huey, R. B., and P. D. Ward (2005), Hypoxia, global warming, and terrestrial late Permian extinctions, *Science*, *308*, 398–401.

Kemp, D. B., A. L. Coe, A. S. Cohen, and L. Schwark (2005), Astronomical pacing of methane release in the Early Jurassic period, *Nature*, *437*, 396–399.

Kiehl, J. T., and C. A. Shields (2005), Climate simulation of the latest Permian: Implications for mass extinction, *Geology*, *33*, 757–760.

Krull, E. S., G. J. Retallack, H. H. Campbell, and G. L. Lyon (2000), $d^{13}C_{org}$ chemostratigraphy of the Permian-Triassic boundary in the Maitai Group, New Zealand: Evidence for high-latitudinal methane release, *N. Z. J. Geol. Geophys.*, *43*, 21–32.

Kump, L. R., A. Pavlov, and M. A. Arthur (2005), Massive release of hydrogen sulfide to the surface ocean and atmosphere during intervals of oceanic anoxia, *Geology*, *33*, 397–400, doi:10.1130/G21295.

Lelieveld, J., F. J. Dentener, W. Peters, and M. C. Krol (2004), On the role of hydroxyl radicals in the self-cleansing capacity of the troposphere, *Atmos. Chem. Phys.*, *4*, 2337–2344.

Levis, S., C. Wiedinmyer, G. B. Bonan, and A. Guenther (2003), Simulating biogenic volatile organic compound emissions in the Community Climate System Model, *J. Geophys. Res.*, *108*(D21), 4659, doi:10.1029/2002JD003203.

Prather, M. J., et al. (2001), Atmospheric chemistry and greenhouse gases, in *Climate Change 2001: The Scientific Basis*, pp. 241–287, Cambridge Univ. Press, New York.

Price, C., and D. Rind (1994), Modeling global lightning distribution in a general circulation model, *Mon. Weather Rev.*, *122*, 1930–1939.

Ramaswamy, V., et al. (2001), Radiative forcing of climate change, in *Climate Change 2001: The Scientific Basis*, pp. 351–416, Cambridge Univ. Press, New York.

Randel, W. J., F. Wu, J. M. Russell III, A. Roche, and J. W. Waters (1998), Seasonal cycles and QBO variations in stratospheric CH4 and H2O observed using UARS HALOE data, *J. Atmos. Sci.*, *55*, 163–185.

Rees, P. M. (2002), Land-plant diversity and the end-Permian mass extinction, *Geology*, *30*, 827–830.

Rozema, J., B. van Geel, L. O. Bjõrn, J. Lean, and S. Madronich (2002), Toward solving the UV puzzle, *Science*, *296*, 1621–1622.

Sassi, F., B. A. Boville, D. Kinnison, and R. R. Garcia (2005), The effects of interactive ozone chemistry on simulations of the middle atmosphere, *Geophys. Res. Lett.*, *32*, L07811, doi:10.1029/2004GL022131.

Schmidt, G. A., and D. T. Shindell (2003), Atmospheric composition, radiative forcing, and climate change as a consequence of a massive methane release from gas hydrates, *Paleoceanography*, *18*(1), 1004, doi:10.1029/2002PA000757.

Seinfeld, J. H., and S. N. Pandis (1998), *Atmospheric Chemistry and Physics*, Wiley-Interscience, Hoboken, N. J.

Sloan, L. C., and D. Pollard (1998), Polar stratospheric clouds: A high latitude warming mechanism in an ancient greenhouse world, *Geophys. Res. Lett.*, *25*, 3517–3520.

Stevenson, D. S., et al. (2006), Multimodel ensemble simulations of present-day and near-future tropospheric ozone, *J. Geophys. Res.*, *111*, D08301, doi:10.1029/2005JD006338.

Twitchett, R. J. (2006), The palaeoclimatology, palaeoecology and palaeoenvironmental analysis of mass extinction events, *Palaeogeogr. Palaeoclimatol. Palaeoecol.*, *232*(2–4), 190–213.

Visscher, H., C. V. Looy, M. E. Collinson, H. Brinkhuis, J. H. A. van Kinijnenburg-van Cittert, W. M. Kürschner, and M. A. Sephton (2004), Environmental mutagenesis during the end-Permian ecological crisis, *Proc. Natl. Acad. Sci. U. S. A.*, *101*, 12,952–12,956.

B. A. Boville, J. T. Kiehl, D. E. Kinnison, J.-F. Lamarque, and C. A. Shields, National Center for Atmospheric Research, 1850 Table Mesa Drive, Boulder, CO 80305, USA. (lamar@ucar.edu)